11. Molecular-Graphics Modelling of the Acid Strength in Zeolites: Influence of the Aluminium Distribution in Offretite

by **Annick Goursot, François Fajula,** and **François Figueras**

Ecole Nationale Supérieure de Chimie de Montpellier, UA418, 8, rue de l'Ecole Normale, F-34075 Montpellier Cedex 2

and **Claude Daul**

Institut de Chimie Inorganique, Université de Fribourg, Boulevard de Pérolles, CH-1700 Fribourg

and **Jacques Weber***

Département de Chimie Physique, Université de Genève, 30 quai Ernest Ansermet, CH-1211 Genève 4

(13.IX.89)

Using extended *Hückel* wave functions, molecular electrostatic potentials (MEP's) have been calculated for several model clusters representative of zeolites of offretite type. The clusters studied, which are all made of a central unit comprising 2 AlO_4 and 16 SiO_4 tetrahedra, differ only by the relative positions of the Al-atoms occupying the same crystallographic sites (T_2) within the zeolite framework. Using the MEP values as a color-coded acidity index for the various clusters, three-dimensional representations of their molecular surfaces are generated as solid models on a performing computer graphics system. Important differences in acidity are predicted for the clusters which can be classified into two types according to the distribution of Al-atoms: the first one is characterized by nearly independent acid sites localized around the main channel of zeolite (*Figs. 3* and *6*), whereas the second one exhibits interacting acid sites located longitudinally along the channel of the same gmelinite cage (*Figs. 4* and *5*). The possible relationship between the structure of the clusters and their catalytic activity towards organic species is discussed.

Introduction. – The activity of the hydrogen forms of aluminosilicate zeolites in acid-catalyzed reactions originates from the presence of protons balancing the negative charges of the AlO_4 tetrahedra. It is well known that the acidity of zeolites is dependent on the number and location of the Al-sites in the framework and that, for Al-rich zeolites, the acid strength of each site increases as the Al-content decreases [1–3].

Offretite is a commonly used acid zeolite, exhibiting the interesting properties to sorb cyclohexane, to convert isoparaffins or decalin, and to show a better efficiency than *ZSM-5* for the dewaxing of gasoils. Our previous study of the acidic properties of this zeolite showed a strong correlation between the acid strength of a site (ability of this site to release a proton) and its local geometry, with an additional influence of the environment [4]. Moreover, the two non-equivalent crystallographic sites of this zeolite (T_1 in hexagonal prisms and T_2 in the six rings of the gmelinite cages (see Fig. 1 in [4])) were predicted to have different acid strengths, in agreement with experiment, with a weaker acidity for the T_1 sites, which are also the most easily dealuminated. These results contribute to a better understanding of the variation of activity of this zeolite as a function of the Al/(Al + Si) ratio m. As it is the case for other zeolites such as mordenite [5] [6] and faujasite [7] [8], the activity of offretite follows a volcano curve, with a maximum for $m = 0.12$ [9].

In addition, our theoretical results have shown that two effects may contribute to the increase of acidity, and subsequently of activity, as m decreases to 0.12: *i*) the sites, which are dealuminated first (T_1) are the less acidic ones and *ii*) the proton efficiency, *i.e.* the ability of the zeolite to release protons, increases simultaneously, as suggested by the examination of the minima of the molecular electrostatic potentials (MEP's) calculated near O-atoms. Indeed, they are predicted to be less attractive when Al-sites become more separated, which suggests that proton-transfer reactions can take place more easily.

It is usually assumed [10] that the maximum of the activity/acidity curve mentioned above corresponds to the highest rate of proton transfer, which remains constant upon a further decrease of m. This point is expected to reflect the situation where there is no more interaction between the acid sites, all of them exhibiting the same maximum efficiency for catalysis. Below this threshold, moreover, the acid strength of each site and the turnover numbers (TON's, indicators of activity per site) should remain constant. In practice, different catalytic behaviors have been reported when varying the turnover numbers in the case of the m ratio lower than the limit value [2] [11] [12]. For offretite, the TON's do not remain constant when $m < 0.12$ [9], but they exhibit an increase or a decrease depending on the reaction studied. This erratic behavior of the TON's led us to investigate whether structural factors could be responsible for such variations.

We have, therefore, decided to perform a theoretical study of different models of offretite where the Al/(Al + Si) ratio is close to 0.12 and with the Al-atoms occupying solely T_2 sites in order to analyze the possible interactions between the acid sites and the variations of their acid strengths with the distribution of the Al-centers. This investigation is based on a combined use of computational quantum chemistry and molecular-graphics techniques.

In a first step, MEP's are calculated for model clusters of these zeolites from extended *Hückel* (EH) wave functions using a method we have derived recently [13]. Then, these MEP's are employed as a local acidity index and mapped according to a color code onto the molecular surfaces of the substrates which allows a good illustration of the results obtained with these large-size and complex clusters.

Method. – A schematic representation of the structure of offretite is presented in *Fig. 1:* there are four different distributions of two Al-atoms in T_2 sites within half of a channel, $T_3T'_3$, T_3T_4, T_4S_4, and $T_4S'_3$. In order to have a structure representative of a value of m close to 0.12, we have chosen four model clusters corresponding to these distributions and made of 2 AlO_4 and 16 SiO_4 tetrahedra *(Fig. 2)*, with the dangling bonds originating from end of chain O-atoms connected to H-atoms. However, to avoid the cases resulting from $Si(OH)_2$ and $Si(OH)_3$ groups as first neighbors of Al-sites, the clusters have been enlarged to 30, 32, or 34 tetrahedra. In addition, in order to compare the results with a reference cluster without any possible interaction between the two Al-sites, a fifth structural model T_4TS has also been studied. All the clusters bear a charge of −2, and their geometry has been taken from a crystallographic study of offretite performed by *Gard* and *Tait* [14].

It is well known [15] that the electrostatic interaction energy $E_{es}(\vec{r})$ (MEP) between a proton and an electronic and nuclear molecular charge distribution is given by:

$$E_{es}(\vec{r}) = \sum_A Z_A/|\vec{r} - \vec{r}_A| - \sum_\mu \sum_\nu P_{\mu\nu} \langle \mu|1/r|\nu\rangle \quad (1)$$

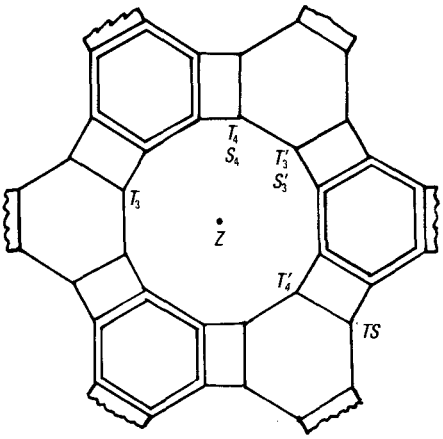

Fig. 1. *Projection of the structure of offretite in (001) plane depicting the main* (central) *channel surrounded by hexagonal cancrinite-* (double stick) *and gmelinite-type* (single stick) *cages.* The $Z(C_3)$ axis is perpendicular to the figure plane. $Z(T_3) = Z(T_4) = Z(T'_3) = Z(T'_4) = Z$; $Z(S_4) = Z(S'_3) = Z - c$; $Z(TS) = Z - 6.0$ Å, with $a = b = 13.29$ Å and $c = 7.58$ Å. For details on the crystal structure, see [14].

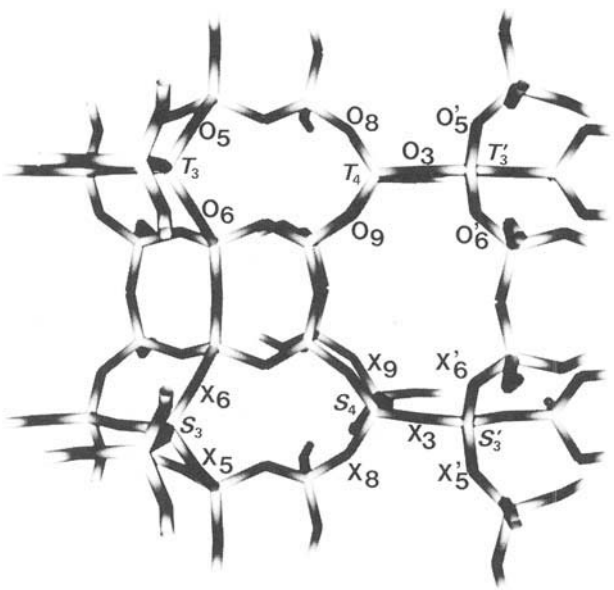

Fig. 2. *Molecular model of a 30-tetrahedra cluster representative of offretite.* The corner-sharing tetrahedra are made of a central Al- or Si-atom (pale end of the stick) linked to oxygen ligands (dark ends of the sticks). T-Type and S-type crystallographic sites are represented with their corresponding O-type and X-type ligands, respectively.

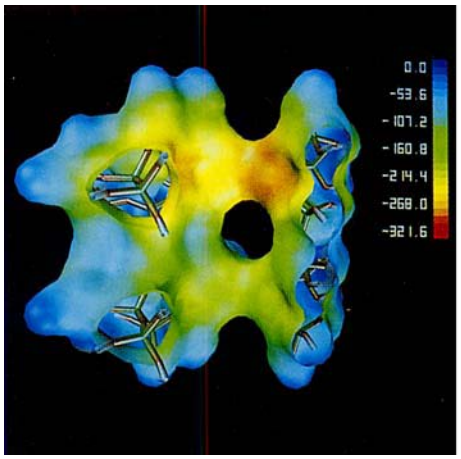

Fig. 3. *Solid model, with partial clipping, of the molecular surface of the* $T_3T'_3$ *cluster, colored according to the MEP value.* The color scale on the right, which is the same for *Figs. 3–6*, indicates the MEP-values [kcal/mol] mapping. The most favorable sites for proton attack correspond to the red zones on the surface.

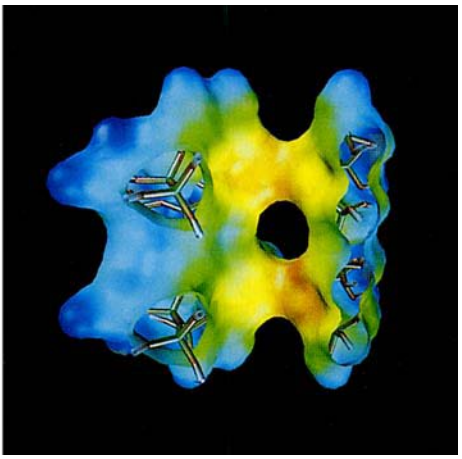

Fig. 4. *Color-coded molecular surface of the* $T_4S'_3$ *cluster.* Conditions, see *Fig. 3.*

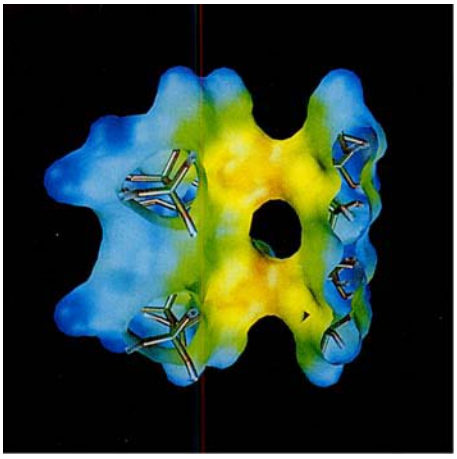

Fig. 5. *Color-coded molecular surface of the* T_4S_4 *cluster.* Conditions, see *Fig. 3.*

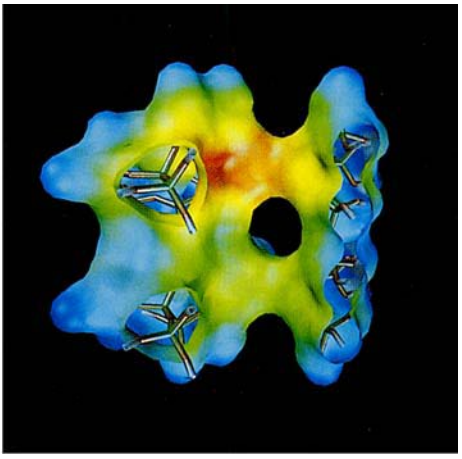

Fig. 6. *Color-coded molecular surface of the* T_3T_4 *cluster.* Conditions, see *Fig. 3.*

where the first term corresponds to nuclear repulsion, the summation running over all atoms with nuclear charge Z_A located in $\vec{r}_A$. The second term describes the electronic attraction, $P_{\mu\nu}$ being the first-order density matrix element corresponding to atomic orbitals (AO's) χ_μ and χ_ν, whereas $\langle\mu|1/r|\nu\rangle$ is defined as:

$$\langle\mu|1/r|\nu\rangle = \int \chi_\mu(\vec{r}') \frac{1}{|\vec{r} - \vec{r}'|} \chi_\nu(\vec{r}') \mathrm{d}\vec{r}' \tag{2}$$

The calculation of $\langle\mu|1/r|\nu\rangle$ integrals using the EH basis of atomic orbitals is time-consuming since they are of *Slater* type [16]. In order to reduce the number of such integrals, we use thus the neglect of diatomic differential overlap (NDDO) approximation, according to which the second righthand term of *Eqn. 1* becomes:

$$\sum_\mu \sum_\nu P_{\mu\nu} \langle\mu|1/r|\nu\rangle = \sum_A \sum_{\mu\varepsilon A} \sum_{\nu\varepsilon A} P_{\mu_A\nu_A} \langle\mu_A|1/r|\nu_A\rangle \tag{3}$$

However, the evaluation of the reduced matrix elements $P_{\mu_A\nu_A}$ is performed using *Löwdin* orthogonalized AO's in order to ensure that the trace of the reduced first-order density matrix is equal to the number of valence electrons of the molecule.

MEP calculations have first been performed for the unprotonated clusters in order to localize the MEP minima and to visualize on the molecular surfaces the variations of acidity due to the relative distributions of Al-centers. However, if one wants to correlate the MEP values with the measured acid strengths per site, it is necessary to carry out another set of calculations with a proton localized on one Al-center. This should lead to a more reliable value for the electrostatic interaction energy between a proton and the second Al-center, and we performed this set of calculations in a second step.

The EH calculations have been carried out using the standard set of parameters [17] without self-consistency of the charge and configuration. In order to display molecular surfaces color-coded according to E_{es} values used as an acidity index, this property is evaluated repeatedly at selected points located on the molecular envelopes of the clusters. Negative (respectively positive) values of E_{es} correspond to attractive (repulsive) interactions. In all cases, the color-coding range from red to yellow to blue extends smoothly over the numerical range of E_{es} from the most negative to zero to the most positive values, which means that the red zones correspond to MEP minima.

Molecular surfaces are generally represented using the dot model suggested by *Connolly* [18]. However, as our clusters are characterized by large sizes and intricate shapes, we have chosen to display the surfaces on the *PS-390* graphics system as more revealing three-dimensional solid models with perspective setting, hidden surface treatment, and smooth shading, obtained by a triangulation algorithm of the dot surfaces recently developed by us [19].

Results. – *Electrostatic Properties of Unprotonated Clusters. Table 1* reports the main features of the MEP's calculated for the unprotonated clusters. Our calculations indicate indeed that several MEP minima are found around each Al-atom, some of them lying at the same depth, and the values reported in *Table 1* for *Case A* correspond to the lowest absolute minima. Roughly speaking, these minima lie generally at a distance of 1 Å from the O-atoms of the corresponding sites. For each cluster, there are four equivalent lowest minima near the AlO_4 tetrahedra and a fifth one is found for the T_3T_4 model. Examination of *Table 1, Case A,* reveals that the clusters with the shortest Al–Al distances exhibit the lowest MEP minima. In addition, a test calculation performed on the same cluster as T_4TS but with a single Al-atom located in T_4 leads, as expected, to the same value for the MEP minimum as T_4TS itself, where the two Al-centers are very far apart (14.3 Å). We can thus conclude that bringing the two Al-centers closer one to the other in the clusters leads to a lowering of the MEP's calculated around each of them which is an illustration of the well-known dilution effect. Actually, the diameter of the main channel of offretite is not very large, as exemplified by the 10-Å distance between two Al-atoms located in T_3 and T'_4 *(Fig. 1)*. In the case of a $T_3T'_4$ cluster, the value of the MEP minimum near T_3 is -325 kcal/mol, which is slightly lower than the value obtained for the cluster with the largest Al–Al distance. However, as a $T_3T'_4$ cluster corresponds to a situation with $m = 0.08$ (2 AlO_4 and 22 SiO_4 tetrahedra), it has not been included in the present investigation.

Table 1. *Characteristics of the MEP's Calculated for Unprotonated Clusters*

Cluster	T_4TS	$T_3T'_3$	$T_4S'_3$	T_4S_4	T_3T_4
Al–Al distance [Å]	14.3	8.9	8.2	7.6	6.9
Case A[b])					
MEP minimum [kcal/mol]	–315	–335	–340	–345	–347
Equivalent O-sites	$O_8O_9(T_4)$	$O_5O_6(T_3)$	$O_8O_9(T_4)$	$O_8O_9(T_4)$	$O_5O_6(T_3)$
(Position of Al-center)		$O'_5O'_6(T'_3)$	$X'_5X'_6(S'_3)$	$X_8X_9(S_4)$	$O_8O_9(T_4)$ MC[a])
Case B[c])					
MEP minimum [kcal/mol]	–270	–293	–300	–295	–315
Equivalent O-sites	$O_8O_9(T_4)$	$O_5O_6(T_3)$	$O_3O_8O_9(T_4)$	$O_3O_8O_9(T_4)$	$O_3O_5O_6(T_3)$
(Position of Al-center)		$O'_5O'_6(T'_3)$	$X_3X'_5X'_6(S'_3)$	$X_3X_8X_9(S_4)$	$O_3O_8O_9(T_4)$ MC[a])

[a]) MC = middle of the cancrinite cage.
[b]) *Case A:* absolute MEP minima within the molecular volume.
[c]) *Case B:* minima on the molecular surface.

The interaction between the zeolite framework and an incoming proton, representative of an electrophilic reactant, may be modeled by the MEP value on the molecular surface for the initial stage of attack [20]; the corresponding results are presented in *Table 1, Case B.* As the points of the molecular envelopes located around O-atoms belong to spheres with radii of 1.5 Å, it is not surprising that the corresponding MEP values are less attractive than those of *Case A.* Due to the shape of molecular surfaces, the balance of attractive and repulsive contributions to the MEP's leads to some changes in the ordering of the minima. The T_3T_4 cluster is now clearly more attractive than the other ones which are practically equivalent. It is also interesting to observe that for the cases with a short Al–Al distance, the number of sites with equivalent minima increases when going from *Case A* to *B.*

The data of *Table 1, Case B,* give only part of the information contained in the color-coded envelopes of our clusters, as it indicates the MEP values calculated at two points. The 3D features of the acidity index calculated for these zeolites could be better appreciated after visualization of the color-coded surfaces by an adequate graphics system. Thus, an immediate correlation between the acid zones on the surface and the structural characteristics of the clusters is possible using our module which allows the display of the molecular model within the properly clipped 3D molecular envelope and the recognition of the boundaries of the acid regions which are all red *(Figs. 3–6).* However, contrasting with recent results obtained for organometallics [19], these most acid zones are spread out over a large region of the surface, which may be ascribed to the simultaneous presence of several MEP minima on the same Al-atom and to the fact that electrostatic interactions reflect the long-range cooperative effects due to the proximity of a second Al-site.

Further examination of *Figs. 3–6* reveals that the clusters may be classified into two types, according to the localization of the acid zones: $T_3T'_3$ and T_3T_4 are characterized by red regions located in the upper part of the surface and spread out around the main channel, whereas $T_4S'_3$ and T_4S_4 exhibit red regions distributed along the main channel of the gmelinite cages. Clearly, this classification of clusters would have been virtually impossible by an examination of the numerical results only. *Figs. 4* and *5* show also an

important delocalization of the acid zone over the whole surface of the gmelinite cage in the $T_4S'_3$ and T_4S_4 clusters, the boundary of the gmelinite channel being also characterized by an acid behavior. Finally, when comparing the separation of the two different acid zones predicted for the clusters, it is seen that $T_3T'_3$ exhibits two distinct regions with little overlap between them. This feature could be related to the largest Al–Al distance characterizing this cluster.

Electrostatic Properties of Protonated Clusters. The results obtained for unprotonated clusters have shown that each AlO_4 tetrahedron has two most attractive and equivalent O-atoms in *Case A* and two or three in *Case B*. In order to correlate the MEP values with the measured acid strengths per site, a proton has been located in turn on each equivalent O-atom, and a new MEP has been calculated for each cluster. The minima of these new MEP's have been sought near the O-atoms of the other AlO_4 center, and the results corresponding to the lowest minima are presented in *Table 2*. As in *Table 1*, a distinction has been made between the absolute MEP minima *(Case A)* and the MEP minima of the molecular surface *(Case B)*. The main difference between corresponding values of *Tables 1* and *2* arises through a repulsive term between the additional H-atom and the incoming proton used to calculate the MEP. This repulsion is expected to be the largest when the distance between the MEP minima of different Al-centers is the shortest in the unprotonated clusters. This positive term is thus the largest for T_3T_4 which exhibits the shortest Al–Al distance, this stronger repulsion balancing the large attractive character reflected by the MEP of *Table 1*. The presence of the additional H-atom leads then to a smaller difference between each cluster and T_4TS. Because of a larger distance between the additional H-atom and the positive charge, this repulsive term is less important on the molecular surface *(Table 2, Case B)*.

It is seen from *Table 2* that for both *Case A* and *B* clusters corresponding to different Al-distributions give rise to different MEP minima, which suggests that their acid strengths are not the same. The differences Δ between the different MEP minima and that of the T_4TS case (independent Al-centers) appear to be either negative but very close to zero (T_3T_4, $T_3T'_3$) or clearly negative (T_4S_4, $T_4S'_3$). The former cases correspond thus to

Table 2. *Characteristics of the MEP's Calculated for Protonated Clusters*

Cluster	T_4TS	$T_3T'_3$	$T_4S'_3$	T_4S_4	T_3T_4
Case A[a])					
Protonated O-sites	X'_7 X'_7	O'_6 O'_5	X'_6	X_8	O_5 O_6
MEP on O-site	O_8 O_9	O_5 O_6	O_8	O_8	O_8 O_9
MEP minimum [kcal/mol]	–290	–295	–310	–315	–290
Δ[b])	–	–5	–20	–25	0
Case B[c])					
Protonated O-sites	X'_7 X'_7	O'_6 O'_5	X'_6	X_9 X_8	O_6
MEP on O-site	O_8 O_9	O_5 O_6	O_8	O_8 O_9	O_3
MEP minimum [kcal/mol]	–240	–245	–270	–265	–245
Δ[b])	–	–5	–30	–25	–5

[a]) *Case A:* absolute MEP minima within the molecular volume.
[b]) Δ = MEP difference with the T_4TS case (non-interacting Al-sites).
[c]) *Case B:* minima on the molecular surface.

two very weakly interacting sites, while the latter ones are characterized by a larger attraction between O-atoms and the incoming proton than in a structure with independent Al-centers. They should, therefore, correspond to less acid materials. Interestingly though the MEP minima of *Case B* are less negative than those of *Case A*, their Δ differences are slightly larger which may be related to variations of the interaction between acid centers with the position of the incoming proton on the molecular surface.

Discussion. – The present results show that, even for an Al/(Al + Si) ratio close to the limit value 0.12, clusters corresponding to various Al-distributions located in T_2 sites within the offretite framework are non-equivalent. In addition, they are characterized by a weak or substantial interaction of their acid sites, depending on the relative positions of the Al-centers, which allows to classify the clusters into two groups. The first one, corresponding to Al-atoms distributed on a ring around the main channel, exhibits nearly independent acid sites. The second one, characterized by Al-centers located longitudinally along the channel of the same gmelinite cage, shows a substantial interaction between acid sites.

It is tempting to correlate the results obtained for the two classes of clusters with the acid strengths of these materials. In the first group of clusters, the acid strength per site should remain nearly constant upon dealumination, whereas an increase of acid strength may be predicted for the second group.

It is well known that, in addition to shape selectivity, the Al-distribution within the zeolite framework plays a role in catalysis, even when the Al-atoms accomodate the same type of crystallographic sites. It is thus probable that typical arrangements of Al-atoms are more favorable for a given reaction. Experimentally, it has been reported that the acid strength of offretite remains nearly constant for benzene ethylation as m decreases, while it increases for toluene disproportionation [9]. This behavior could be related to the fact that, due to their size, toluene molecules interact with acid sites located longitudinally along the channel, while benzene and EtOH molecules are sufficiently small to interact also with acid sites situated around the channel (the volume available in the main channel of offretite has a diameter of 6.2 Å). Such a conclusion is indeed speculative and would deserve confirmation, but in any case, our results validate the assumption that, at the optimum value of m and for identical crystallographic sites, the distribution of AlO_4 tetrahedra within the zeolite framework affects the acid strength of each site.

A final comment may concern the theoretical model used in this study. An investigation of the influence of the Al-distribution on the acid properties of zeolites necessitates to model the materials using very large clusters containing over 100 atoms. This means that the quantum-chemical method employed to derive their physico-chemical properties must be approximate, though leading to meaningful results. We have found in this respect that wave functions calculated from the EH method may be used to evaluate MEP's which lead to a satisfactory description of the electrostatic properties of compounds such as zeolites or organometallics. In view of both the large size and intricate shape of clusters representative of zeolites, the combination of molecular graphics and computational quantum chemistry approaches provides a comprehensive perception of the main features of the calculated properties.

The presented method leads to a simplified description of intermolecular forces between the material and the incoming reactant, which means that it is intended to predict

the initial stage of attack only. However, our results suggest that it is suitable for a rationalization of the acid properties of zeolites framework. Further work aiming at describing along these lines the reactions taking place in zeolite channels is in progress.

We are grateful to Dr. *P. Y. Morgantini* and Mr. *P. Fluekiger* for their assistance. The calculations have been performed at the *CNUSC* in Montpellier and at the Computer Center of the University of Geneva. This work has been supported by the *Swiss National Science Foundation.*

REFERENCES

[1] D. Barthomeuf, *J. Phys. Chem.* **1979,** *83,* 249.
[2] D. Barthomeuf, R. Beaumont, *J. Catal.* **1973,** *30,* 288.
[3] D. Freude, M. Hunger, H. Pfeifer, *Chem. Phys. Lett.* **1986,** *121,* 62.
[4] A. Goursot, F. Fajula, C. Daul, J. Weber, *J. Phys. Chem.* **1988,** *92,* 4456.
[5] S. Namba, H. Hosonuma, Y. Yashima, *J. Catal.* **1981,** *72,* 16.
[6] F. Fajula, R. Ibarra, F. Figueras, C. Gueguen, *J. Catal.* **1984,** *89,* 60.
[7] R. Vetrivel, C. R. A. Catlow, E. A. Colbourn, *Stud. Surf. Sci. Catal.* **1988,** *37,* 317.
[8] K. Tsutsumi, H. Tokahashi, *J. Catal.* **1972,** *24,* 1.
[9] F. Fajula, M. Lambret, F. Figueras, *Stud. Surf. Sci. Catal.* **1989,** *46,* 61.
[10] D. Barthomeuf, *Mater. Chem. Phys.* **1987,** *17,* 49.
[11] S. J. De Carrio, J. R. Sohn, P. O. Fritz, J. H. Lunsford, *J. Catal.* **1986,** *101,* 132.
[12] A. Corma, in 'Physicochemical Properties of Zeolitic Systems and Their Low Dimensionality', Eds. D. Barthomeuf, E. G. Derouane, and W. Hoelderich, Plenum Press, New York, 1989, in press.
[13] J. Weber, P. Fluekiger, P. Y. Morgantini, O. Schaad, A. Goursot, C. Daul, *J. Comp. Aid. Mol. Design* **1988,** *2,* 235.
[14] J. A. Gard, J. M. Tait, *Acta Crystallogr., Sect. B* **1972,** *28,* 825.
[15] E. Scrocco, J. Tomasi, *Adv. Quantum Chem.* **1978,** *11,* 121.
[16] R. Hoffmann, *J. Chem. Phys.* **1963,** *39,* 1397.
[17] J. Howell, A. Rossi, D. Wallace, K. Haraki, R. Hoffmann, *QCPE Bull.* **1979,** *11,* 344.
[18] M. L. Connolly, *Science* **1983,** *221,* 709.
[19] J. Weber, P. Fluekiger, A. Ricca, P. Y. Morgantini, in 'Visualisierungstechniken und Algorithmen', Ed. H. Barth, Springer, Berlin, 1988, pp. 17–30.
[20] J. Weber, P. Fluekiger, P. Y. Morgantini, *Ann. Soc. Sci. Bruxelles,* in press.